JOURNAL OF CATALYSIS 155, 1–11 (1995)

Isomerization of *n*-Heptane over Pd-Loaded Silico-Alumino-Phosphate Molecular Sieves

B. Parlitz,* E. Schreier,† H.-L. Zubowa,* R. Eckelt,* E. Lieske,† G. Lischke,‡ and R. Fricke*,[1]

*Institut für Angewandte Chemie, Adlershof, Rudower Chaussee 5, 12484 Berlin, Germany; †Humboldt-Universität Berlin, Hessische Str. 1, 10115 Berlin, Germany; and ‡Technische Fachhochschule Wildau, Friedrich-Engels-Str. 63, 15742 Wildau, Germany

Received January 4, 1994; revised February 1, 1995

Isomerization of *n*-heptane was studied on a series of bifunctional SAPO-based catalysts with contents of 0.1 wt% Pd. From results on temperature programmed desorption of NH_3 it is deduced that the different molecular sieve structures contain nearly identical amounts of silicon substituting for phosphorus in the framework (0.3 to 0.5 silicon atoms per unit cell). Best activities and selectivities for branched heptane isomers are achieved with SAPO-11 and SAPO-31. SAPO-17 and SAPO-5 show substantially lower activities. With SAPO-5, there is a high cracking selectivity which is assumed to be caused by the reduced accessibility of parts of the bridged hydroxyl groups within the molecular sieve framework. Different locations of these acid sites are evidenced by infrared OH vibration spectra recorded after adsorption of *n*-heptane. © 1995 Academic Press, Inc.

INTRODUCTION

The transfer of normal paraffinic hydrocarbons into branched isomers is a matter of constant industrial interest. At present, this conversion is gaining attraction in the field of catalytic dewaxing of hydrocarbon feedstocks (1).

The isomerization of *n*-alkanes on bifunctional metal acid catalysts in a multistep reaction proceeding consecutively on the metallic and the acidic catalytically active sites (2). The activity and selectivity of the reaction are strongly influenced by the acidic and structural properties of the catalyst (2–9). It has been reported earlier that with catalysts based on molecular sieves, the distribution of isomers is influenced by the width of the pores and of the cavities of the molecular sieve framework. In general, it is assumed that methyl branching is favored with decreasing pore width, whereas ethyl- and propyl-branched isomers require wide pore openings and large cavities. Thus in the isomerization of *n*-dodecane over ZSM- and Y-type zeolites, ethyl-decanes are only produced in molecular sieve structures with pores or cavities formed by at least 12-membered oxygen rings. The formation of propyl-nonanes requires both 12-membered pore openings and large cavities (6, 10, 11). As was demonstrated by the results of the isomerization of *n*-hexane and *n*-heptane (4), the distribution among the alkane isomers is also influenced by the numerical ratio between metallic and acidic sites and their relative activities. The formation of multibranched isomers depends on the probability of the *n*-olefin that results from the dehydrogenation of the *n*-alkane on a metallic site encountering enough active acid sites to undergo successive isomerization into a di- or tribranched olefin before being hydrogenated on another metallic site, as opposed to isomerization being stopped at the monobranched olefin.

However, the application of the conclusions drawn from the results of one series or class of molecular sieves to another might be somewhat problematic. Due to the differences in the shape of the pores, more or less pronounced pecularities of the kind of interaction between the reactants and the active sites can be expected.

The aim of the present paper is to investigate the influence of the different pore structures of SAPO-type molecular sieves on the isomerization of *n*-heptane. The catalysts contain Pd as the metallic component. For reasons of comparison, the investigation was extended to the corresponding $AlPO_4$ species.

EXPERIMENTAL

Synthesis of the Molecular Sieves

The synthesized and investigated types of molecular sieves are listed in Table 1.

Synthesis is based on the method described by Lok *et al.* (12), including some variations of the procedure outlined earlier (13). Orthophosphoric acid, silica sol (containing 30 wt% SiO_2) and pseudo-boehmite (AEL- and ATO-structures), aluminum oxide hydrate sol (AFI structures), or aluminum isopropoxide (ERI structures) were

[1] To whom correspondence should be addressed.

0021-9517/95 $12.00

TABLE 1

Structure Type, Size, and Molecular Weight of the Unit Cells of Investigated Samples

Sample	Structure type	Size of unit cell	Molecular weight of unit cell (g/mol)	Content of unit cells per mass unit of molecular sieve (mmol/g)
SAPO-17; $AlPO_4$-17	ERI	$Al_{18}P_{18}O_{72}$	2195.3	0.455
SAPO-11; $AlPO_4$-11	AEL	$Al_{20}P_{20}O_{80}$	2439.2	0.410
SAPO-31; $AlPO_4$-31	ATO	$Al_{18}P_{18}O_{72}$	2195.3	0.455
SAPO-5; $AlPO_4$-5	AFI	$Al_{12}P_{12}O_{48}$	1463.5	0.683

used as P, Si, and Al sources. Triethylamine (TEA), di-*n*-propylamine (Pr_2NH), and cyclohexylamine (CHA) were the templating agents for AFI, AEL, and ATO and ERI structures, respectively. The ATO molecular sieves were synthesized using $AlPO_4$-31 as seed crystals. The synthesis of the $AlPO_4$ types was based on the corresponding silica sol-free gels.

Methods of Characterization

XRD. XRD powder diffraction patterns were recorded in the range $2.2° < \theta < 20°$ with the aid of a Bragg–Brentano diffractometer fitted with a source for Cu$K\alpha$ radiation.

Adsorption/desorption. The isotherms of *n*-hexane adsorption/desorption were recorded at 293 K. The micropore volumes were estimated by means of the Dubinin–Radushkevich plots (14) of the adsorption/desorption data.

IR Spectroscopy

IR spectra were recorded by an M 85 Specord Instrument (Carl Zeiss, Jena). The self-supporting wafers of the molecular sieve samples (7 mg/cm^2) were placed in a quartz IR cell and activated by heating to 673 K under vacuum. To characterize the acidity of the Brønsted sites, ammonia and *n*-heptane were adsorbed at room temperature. Adsorption was followed by evacuation at room temperature to remove any physically adsorbed molecules. Stepwise desorption of ammonia was carried out from room temperature up to 573 K. IR spectra were recorded at room temperature in the ranges 3800–3200 cm^{-1} and 1800–1300 cm^{-1}.

Temperature Programmed Desorption

Prior to temperature programmed desorption of ammonia (TPDA), the samples (500 mg of the granulated substance) were cleaned by heating to 773 K in a stream of helium ($\dot{v}$ = 1 ml/s) for 1 h. Subsequently, ammonia was adsorbed at 393 K from a helium gas flow containing 3 vol% NH_3. After 2 h of flushing with pure helium at 393 K to remove physically adsorbed ammonia, TPDA up to 773 K was started in a stream of helium (1 ml/s) with a heating rate of 10 K/min. The concentration of ammonia in the exit gas was determined using a thermoconductivity cell.

Catalysis

Catalytic experiments were performed in a flow type reactor with 10 ml cylindrically shaped catalyst pellets (diameter 1.5 mm) containing 65 mass% of molecular sieve powder bound with Aerosil-200. To obtain bifunctional catalysts with 0.1 mass% of Pd, the pellets were impregnated with an aqueous solution of $(Pd(NH_3)_4)Cl_2$, dried, calcined in air at 620 K, and finally reduced in a stream of hydrogen. The conditions of the catalytic reaction are listed in the notes to Tables 7 and 8, which present the catalytic results. Analysis of the products of reaction was based on an on-line coupled gas-chromatographic device. Selected liquid samples of the product were analyzed by off-line capillary gas chromatography.

RESULTS AND DISCUSSION

Characterization

For the SAPO samples, the compositions of the gel mixtures, along with the results of the standard wet chemical analysis and the micropore volumes, are given in Table 2.

For all molecular sieves used in our experiments, XRD patterns (Fig. 1) coincide with the data given in the literature (12, 15). With $AlPO_4$-31 and SAPO-31, additional reflections at d = 0.884, 0.547, 0.444, and 0.375 nm point to the presence of an alien AEL structure type phase.

The intensity of XRD lines, which is a measure of the crystallinity of the recorded samples, has the highest values with SAPO-5. To evaluate the degree of crystallinity, the intensities of the lines of the spectra of the other samples are related to that of the characteristic line of SAPO-5 at d = 1.195 nm, which is set arbitrarily to 100%. Intensity values (units of the ordinate of Fig. 1) reveal

TABLE 2

Analytical Composition and Micropore Volumes of SAPO Samples

Sample	Composition of the synthesis gel (mole ratios)	Chemical analysis (atomic ratios) Al : P : Si	Micropore volume (cm^3/g)
SAPO-17	1.0 CHA : 1.0 Al_2O_3 : 1.0 P_2O_5 : 0.1 SiO_2 : 50 H_2O	1.04 : 1 : 0.06	0.087
SAPO-11	1.0 Pr_2NH : 1.2 Al_2O_3 : 1.0 P_2O_5 : 0.1 SiO_2 : 40 H_2O	1.28 : 1 : 0.05	0.073
SAPO-31	1.0 Pr_2NH : 1.2 Al_2O_3 : 1.0 P_2O_5 : 0.1 SiO_2 : 50 H_2O	1.41 : 1 : 0.13	0.078
SAPO-5	1.0 TEA : 1.0 Al_2O_3 : 2.4 P_2O_5 : 0.1 SiO_2 : 300 H_2O	1.06 : 1 : 0.10	0.090

that in decreasing sequence of crystallinity, SAPO-5 is followed by SAPO-17; SAPO-31 and SAPO-11 show the lowest values.

The isotherms of *n*-hexane adsorption/desorption exhibit hysteresis loops indicating the existence of mesopores (Fig. 2). The micropore volumes (Table 2) of SAPO-5 and SAPO-17 exceed those observed with the medium pore molecular sieves SAPO-11 (elliptical pore aperture of 0.39 × 0.63 nm) and SAPO-31 (tilted circular pore apertures of 0.54 nm) by 15 to 19%. The high value of SAPO-5 is obviously caused by its wide 0.73-nm circular pore apertures. In the case of SAPO-17 (elliptical pore apertures of 0.36 × 0.51 nm), the large micropore volume is apparently caused by the two large cages (1.51 × 0.63 nm) characteristic of its unit cell (15). The small differences in the micropore volumes of SAPO-31 and SAPO-11 may indicate that the circular pore apertures (SAPO-31) are slightly more suitable for *n*-hexane uptake.

As reported earlier (16), the replacement of phosphorus by silicon in the AEL structure type may be problematic. The ^{29}Si MAS NMR spectrum of SAPO-11 synthesized as described above exhibits two signals, one at −89.1 ppm and a weaker one at −112 ppm, proving that more than one type of silicon is present in this sample. The signal at −112 ppm is consistent with Si linked to neighboring Si atoms (17). The more intense line at −89.1 ppm

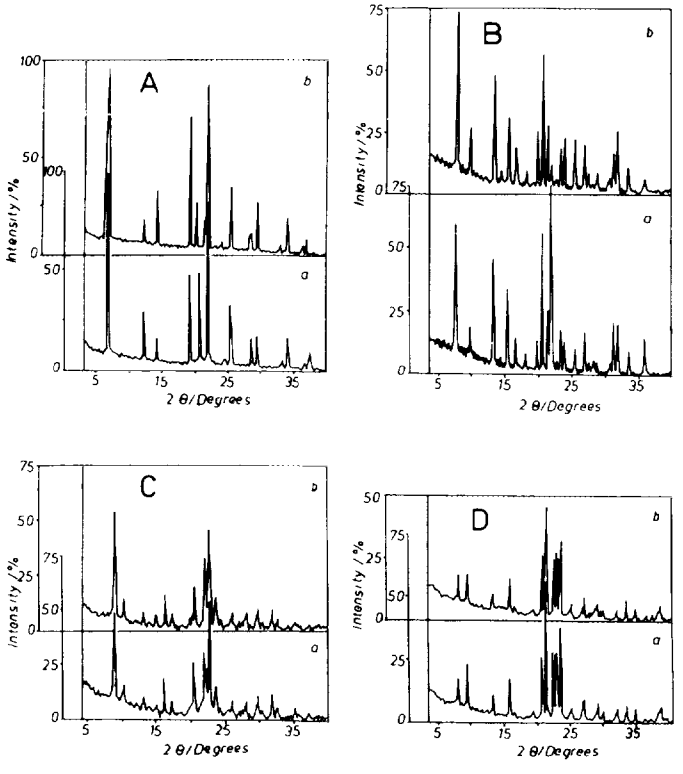

FIG. 1. XRD patterns of SAPO and $AlPO_4$ samples: A, SAPO-5 (AFI) (a) and $ALPO_4$-5 (b) after calcination at 873 K; B, SAPO-17 (ERI) (a) and $AlPO_4$-17 (b) (as synthesized); C, SAPO-31 (ATO) (a) and $AlPO_4$-31 (b) calcined at 873 K; D, SAPO-11 (AEL) (a) and $AlPO_4$-11 (b) (as synthesized).

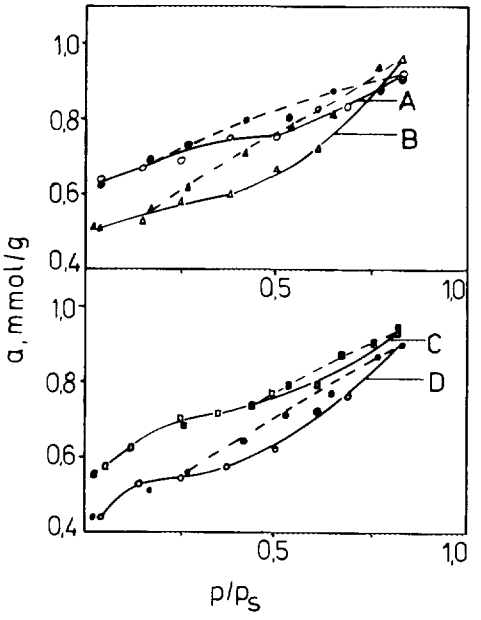

FIG. 2. Adsorption isotherms of *n*-hexane on SAPO-11 (A), SAPO-5 (B), SAPO-31 (C), and SAPO-17 (D), with broken lines denoting the desorption branches.

can be attributed to Si(4Al) units formed by substitution of Si for a single P of the $AlPO_4$ framework. Similar assignments of lines in the −90 ppm region have been suggested for SAPO-11 (18), SAPO-5 (17), and SAPO-31 (13).

It is known from the literature (19) that, depending on the conditions of synthesis, SAPO-5 may form microcrystallites of larger size. Microscopy, however, proves that the SAPO-5 sample under investigation consists of spherical agglomerates of small microcrystallites similar to those obtained in the synthesis of SAPO-11. The diameter of the agglomerates does not exceed 1 μm.

IR Spectroscopy

Figure 3 shows the IR spectra of the SAPO and the corresponding $AlPO_4$ samples recorded in the range of OH vibrations. With the SAPOs, four characteristic bands are detected at 3740 and 3676 cm^{-1} and in the regions of 3616/3628 and 3524/3592 cm^{-1}. According to the literature (20, 21) they are assigned to OH vibrations of terminal Si–OH (3740 cm^{-1}), of P–OH (3676 cm^{-1}), and of bridging SiOHAl groups (3616/3628 and 3524/3592 cm^{-1}). As was demonstrated in the case of SAPO-31 (13), P–OH groups can be ascribed to phosphorus atoms not fully linked to AlO_4 tetrahedra. Si–OH groups are located at the outer zeolite surface area or belong to amorphous silica impurities of the samples. The double bands of SiOHAl vibration are indicative of two different kinds of SiOHAl acid groups. The band at 3616/3628 cm^{-1} is assigned to undisturbed bridged OH groups whereas the one at 3592/3524 cm^{-1} can be attributed to bridge OH groups interacting with the oxygen atoms of the framework (21, 22). As

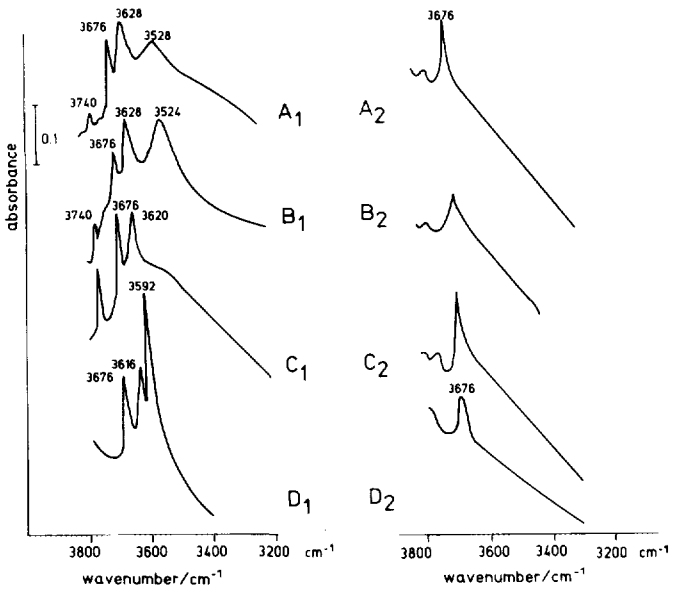

FIG. 3. OH vibration spectra of the SAPO and $AlPO_4$ samples: (A_1) SAPO-11, (A_2) $AlPO_4$-11, (B_1), SAPO-5, (B_2) $AlPO_4$-5, (C_1) SAPO-31, (C_2) $AlPO_4$-31, (D_1) SAPO-17, (D_2) $AlPO_4$-17.

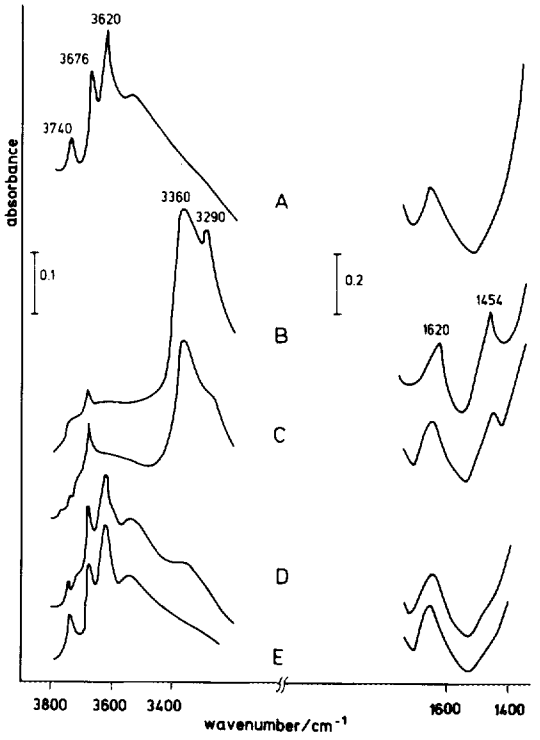

FIG. 4. IR spectra of SAPO-31 recorded before and after adsorption of ammonia: (A) initial spectrum, (B) spectrum recorded after adsorption of ammonia followed by 18 h desorption in vacuum at room temperature, (C) after desorption at 373 K, (D) after desorption at 473 K, (E) after desorption at 573 K.

expected, the bands caused by the presence of silicon in the framework are completely absent in all of the $AlPO_4$ spectra (Fig. 3).

IR spectra recorded following the adsorption of ammonia at room temperature and an 18-h treatment in vacuum to remove physically adsorbed ammonia (Fig. 4, curve B) show that the bands characteristic of the OH vibrations of the SiOHAl groups have completely vanished. The two bands which correspond to P–OH (3676 cm^{-1}) and Si–OH (3740 cm^{-1}) are distinctly decreased. Simultaneously, new bands appear at 3360 and 3290 cm^{-1}. They can be assigned to N–H stretching vibrations of NH_4^+ with NH_3, respectively (23). The new bands in the region of lower wavenumbers are attributed to deformation vibrations of NH_3 (1620 cm^{-1}) and NH_4^+ (1454 cm^{-1}). NH_4^+ bands originate from ammonium ions formed by the interaction of ammonia and Brønsted acid groups. The band at 1620 cm^{-1}, which partially overlaps the structure band at 1640 cm^{-1}, is assigned to NH_3, probably adsorbed coordinatively at Lewis sites.

Desorption of ammonia by a stepwise temperature increase results in a clear reduction of the intensities of the band at 1454 cm^{-1}. Whereas the bands assigned to SiOH and POH groups reachieve their original intensity after desorption at 373 K, the bands of bridged OH groups

remain absent. They appear only after treatment at 473 K. Finally, after desorption at 573 K the original spectrum of OH vibration is completely restored and all bands in the low region of wavenumbers have vanished (Fig. 4, curves C and D). No differences in the behavior of the two types of bridged OH groups can be detected. Their acidic strengths are assumed to be identical.

The normalized intensities of the band assigned to deformation vibrations of NH_4^+ (Table 3) are related to the number of Brønsted acid sites (P–OH and SiOHAl). As expected, the acidity of the SAPOs is substantially higher than that of the corresponding $AlPO_4$s. Values after desorption at 373 K (which then can be related to the bridged SiOHAl groups of the framework only) show that differences in their number can be neglected. The correlation between the intensity of deformation vibrations of NH_4^+ and the number of Brønsted acid sites is supported by the results of TPDA found with our samples and presented in the next section.

The deviations in the temperatures of desorption within the series are small, indicating that differences in the binding strength of ammonia are not substantial. Hence, the acidic strength of the Brønsted sites can be considered nearly identical.

The relative amount of weaker Brønsted acidities which cannot be related to the SiOHAl groups of the framework (Figs. 3 and 4) and which apparently originate from P–OH groups can be estimated from the differences in the intensities of NH_4^+ deformation vibrations (1454 cm^{-1}) recorded after brief evacuation at room temperature and after desorption at 373 K (Table 3). The values given in Table 4 do not reveal significant differences within both series. The slightly higher values found with SAPO-17 and SAPO-5 may indicate that imperfections within the structure of their frameworks are more numerous, thus giving rise to higher concentrations of P–OH groups.

To characterize the accessibility of hydroxyl groups, comparison of IR spectra after adsorption of molecules of different size and basicity can be helpful. Ammonia molecules are able to interact with most of the OH groups present in the investigated SAPOs (Fig. 4). After adsorption of *n*-heptane, however, only the OH groups at 3616/3628 cm^{-1} are covered; intensities of the bands at 3524/3592 cm^{-1} remain unaffected (Fig. 5). Similar effects are reported with IR spectra of SAPO-5 after adsorption of benzene (24) and with H–MAS NMR spectra recorded after adsorption of perdeuterated cyclohexane (22). Differences in the interaction of hydroxyl groups with larger and less basic molecules are interpreted in terms of different locations. Bands at 3616/3628 cm^{-1} are assigned to the more easily accessible groups within the main channels, whereas the bands in the lower region of wavenumbers are attributed to groups outside the main channels located in the six-membered rings of the framework. Either they are not accessible to the *n*-heptane molecules or the basicity of *n*-heptane is not high enough to attract OH vibrating at 3524/3592 cm^{-1} into large cavities or channels. IR vibration spectra (Fig. 3) demonstrate that the relative portion of bridged hydroxyl groups (3524/3592 cm^{-1}) unable to interact with *n*-heptane is substantially larger with SAPO-17 and SAPO-5 than it is with SAPO-11 and SAPO-31.

TABLE 3

Relative Intensities (Arbitrary Units) of the Maxima of the IR Bands at 1620 cm^{-1} (NH_3) and at 1454 cm^{-1} (NH_4^+) Normalized on a 30-mg Pellet

	SAPO-17		SAPO-11		SAPO-5		SAPO-31	
	NH_3	NH_4^+	NH_3	NH_4^+	NH_3	NH_4^+	NH_3	NH_4^+
Pretreatment	1620 cm^{-1}	1454 cm^{-1}	1620 cm^{-1}	1454 cm^{-1}	1620 cm^{-1}	1454 cm^{-1}	1620 cm^{-1}	1454 cm^{-1}
30 min vacuum, room temp.	0.43	0.76	0.23	0.60	0.00	0.70	0.18	0.57
18 h vacuum, room temp.	0.17	0.58	0.09	0.45	0.00	0.70	0.08	0.47
30 min vacuum, 373 K	0.08	0.44	0.00	0.36	0.00	0.30	0.05	0.36
30 min vacuum, 473 K	0.00	0.11	0.00	0.07	0.00	0.05	0.00	0.07
30 min vacuum, 573 K	0.00	0.00	0.00	0.00	0.00	0.00	0.00	0.00
	$AlPO_4$-17		$AlPO_4$-11		$AlPO_4$-5		$AlPO_4$-31	
	NH_3	NH_4^+	NH_3	NH_4^+	NH_3	NH_4^+	NH_3	NH_4^+
30 min vacuum, room temp.	0.19	0.23	0.23	0.20	0.00	0.11	0.15	0.19
18 h vacuum, room temp.	0.09	0.16	0.11	0.11	0.00	0.08	0.07	0.12
30 min vacuum, 373 K	0.00	0.08	0.06	0.04	0.00	0.00	0.04	0.06
30 min vacuum, 473 K	0.00	0.00	0.00	0.00	0.00	0.00	0.00	0.00

TABLE 4

Relative Intensities of P–OH Groups, Estimated from the Differences between the Intensities of the NH_4^+ Bands Recorded after Pretreatment at Room Temperature and at 373 K (Values of Table 3)

SAPO-17	0.32
SAPO-11	0.24
SAPO-5	0.40
SAPO-31	0.21

Temperature Programmed Desorption of Ammonia

Ammonia can interact with Lewis and Brønsted sites of different acidic strengths. In the TPDA spectra, the low temperature NH_3 peak with its maximum around 470 K is generally attributed to weak (Brønsted or Lewis) acid sites, whereas desorption proceeding at higher temperatures (510 to 525 K) is attributed to stronger acid (Brønsted) sites (25).

With the $AlPO_4$ molecular sieves, only weak acid (Lewis and Brønsted) sites of P–OH groups are able to adsorb ammonia. The amount of desorbed ammonia is small and desorption is complete at low temperatures with a peak maximum at about 470 K (Fig. 6). The situation is clearly different with the silicon-containing SAPOs. The amounts of adsorbed ammonia are substantially higher and the TPDA profiles exhibit two maxima, pointing to the existence of at least two types of adsorbing sites of different acidic strengths. Desorption at higher temperatures is attributable to the strong acid sites generated by the incorporation of silicon into the framework of the molecular sieve (26).

Shifts in the position of the high temperature maximum cannot necessarily be related to differences in the acidic strength of the SiOHAl sites. They might be caused by influences of the individual width of the pores and the structure of the void volume of the different types of the molecular sieve on the diffusion of the desorbing ammonia.

Quantitative estimation of the amount of ammonia desorbed at higher temperatures can be based on three procedures:

(i) graphical separation of the total area of desorption following ammoniation at 393 K into a low and a high temperature region,

(ii) stepwise TPDA interrupted by isothermal periods and independent integration of the areas under the desorption curves separated this way, or

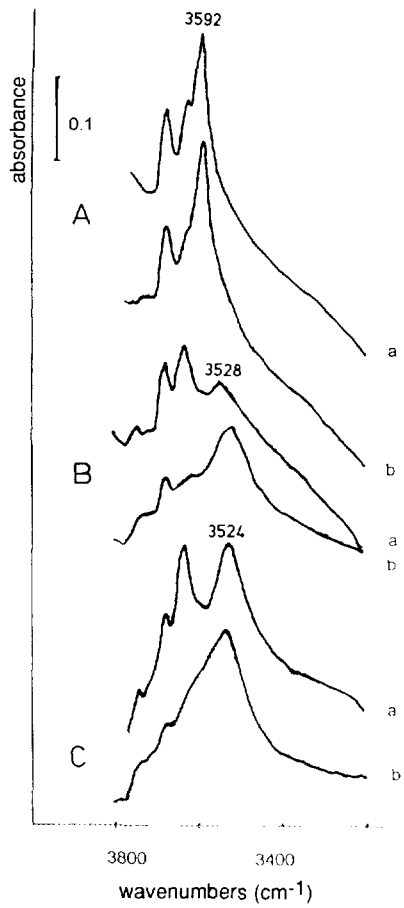

FIG. 5. IR vibration spectra recorded before (a) and after (b) adsorption of *n*-heptane: (A) SAPO-17, (B) SAPO-11, (C) SAPO-5.

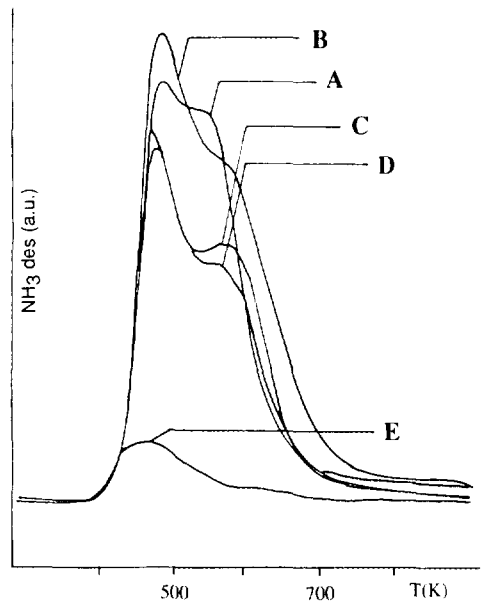

FIG. 6. TPDA curves after adsorption of ammonia at 393 K: (A) SAPO-5, (B) SAPO-17, (C) SAPO-11, (D) SAPO-31, (E) $AlPO_4$-5.

(iii) adsorption at a higher temperature prior to TPDA, thus limiting coverage by ammonia to the strong acid Brønsted sites only.

A further TPDA method of determining Brønsted sites is offered by the deammoniation of the NH_4^+ form of molecular sieves obtained by ammonium exchange in diluted liquid solutions of ammonium salts (27).

Method (i) is a variety of the traditional interpretation of desorptive or chromatographic profiles. The reliability of its results depends on the quality of the separation of the different species. The experimental procedures of methods (ii) and (iii) are rather extensive. The right moment to stop the temperature programmed desorption and to continue isothermally (method (ii)) has to be determined by independent runs for any of the samples. Similarly, previous runs are necessary to find the optimum temperature of adsorption, where coverage of weak Lewis and Brønsted sites by ammonia (method (iii)) is largely excluded and losses of ammonia adsorbed at the strong acid sites are still negligible.

Data (Table 5) show that method (i) (column 3) and method (iii) (column 4) result in nearly identical density values of ammonia adsorbed at the strong acid Brønsted sites. As with many other types of molecular sieves, the separation of the two peaks of ammonia desorbed from the investigated SAPO samples is apparently sufficient for graphical discrimination (method (i)). Likewise, adsorption of ammonia at elevated temperatures (method (iii)) prior to temperature programmed desorption (Fig. 7) proves to be a suitable way of excluding adsorption by the weaker acid sites. The desorbed ammonia then represents the total number of the sites of stronger acidity, provided that the optimal temperature of adsorption of ammonia has been determined carefully in previous runs,

TABLE 5

Temperature Programmed Desorption of Ammonia (TPDA), Densities of Desorbed Ammonia (mmol/g)

Sample	1	2	3	4
SAPO-17	0.52	0.27	0.25	0.23
SAPO-11	0.36	0.17	0.19	0.18
SAPO-5	0.41	0.20	0.21	0.21
SAPO-31	0.34	0.20	0.14	0.14
$ALPO_4$-17	0.12	—	—	—
$ALPO_4$-11	0.11	—	—	—
$ALPO_4$-5	0.05	—	—	—
$ALPO_4$-31	0.09	—	—	—

Note. Column 1: density of total ammonia desorbed after adsorption at 393 K. Column 2: density of ammonia desorbed in the low temperature region after adsorption at 393 K (method (i)). Column 3: density of ammonia desorbed in the high temperature region after adsorption at 393 K (method (i)). Column 4: density of ammonia desorbed after adsorption at 473/508 K (method (iii)).

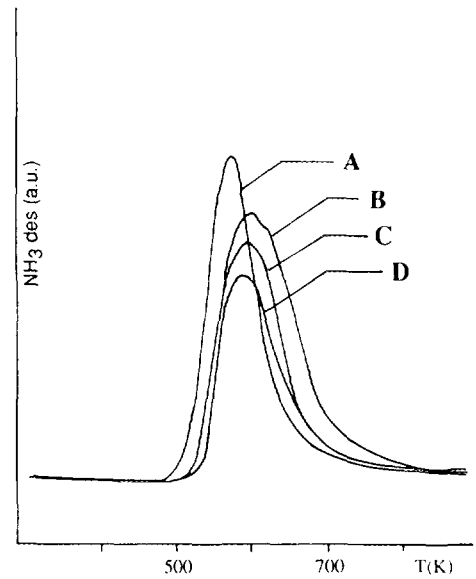

FIG. 7. TPDA curves after adsorption of ammonia at 503 K: (A) SAPO-5, (B) SAPO-17, (C) SAPO-11, (D) SAPO-31.

as is demonstrated for the case of the SAPO-31 sample (Fig. 8).

Preliminary tests have shown that the data for the high temperature desorption of ammonia derived according to method (ii) are comparatively small. The two regions of desorption of ammonia are overlapping. Desorption of parts of the strongly held ammonia during the previous

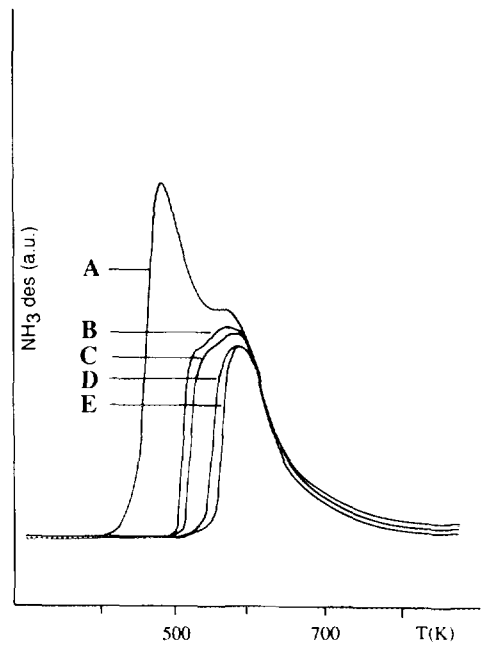

FIG. 8. TPDA curves for SAPO-31. Separation of the high temperature peak following adsorption of ammonia at different temperatures: (A) 393 K, (B) 473 K, (C) 493 K, (D) 508 K, (E) 523 K.

isothermal period (about 120 min) cannot be completely excluded.

Deammoniation of NH_4^+ ion-exchanged SAPO samples has been shown to produce inadequate results. The amount of ammonia desorbed during deammoniation is distinctly higher than that determined by the standard TPDA. Due to the presence of water during the ion exchange in the aqueous solutions of ammonium acetate, the SAPO framework is partially damaged by hydration and the number of hydroxyl groups is drastically increased. The influence of water is confirmed by IR spectroscopy. Depending on the type of SAPO structure, the effect of hydration can be reversible in some cases (SAPO-5 and SAPO-31), whereas in other cases hydration results in an irreversible destruction of the framework of the molecular sieve (SAPO-17, SAPO-34) (28).

According to the data of Table 5 (columns 3 and 4), the molar amounts of ammonia adsorbed per gram of the molecular sieve by the strong SiOHAl acid sites are of the same order of magnitude for any of the SAPO samples. From these density values and the molecular weights of the unit cells of the structure types (Table 1, columns 4 and 5, respectively), the average number of silicon atoms isomorphously substituted per unit cell of the molecular sieve can be calculated (Table 6). Values do not differ substantially and lie in the range between 0.3 and 0.5. As was shown recently (29), the influence of small differences in Brønsted acidities like this on catalytic activities is negligible.

By comparing the composition of the unit cells with the atomic ratios of the elements found by chemical analysis (Table 6), the contents of nonframework silicon and aluminum within the SAPO samples can be estimated. Non-SAPO framework Al_2O_3 and SiO_2, the contents of which are highest with SAPO-31, can be present either in the amorphous state or as domains within the SAPO phases. The relative intensities of the IR bands assigned to coordinatively bound ammonia (Table 3) do not correlate with the estimated contents of non-SAPO oxides (Table 6). This may indicate that, perhaps due to the individual states of agglomeration in different SAPO structures, the adsorptive capacities of these oxides differ greatly.

Catalytic Reaction

Results of the catalytic isomerization of *n*-heptane are shown in Tables 7 and 8. The level of conversion is the highest with SAPO-11 and SAPO-31. The lowest degree of conversion is achieved with SAPO-17, which is characterized by the smallest pore apertures. As expected, $AlPO_4$ catalysts, the Brønsted acidity of which originates from P–OH groups of comparatively low acidic strength only, show a substantially lower activity than those based on the SAPOs. The highest selectivities for the desired products, the branched heptane isomers, are found with SAPO-11 and SAPO-31. The selective behavior of SAPO-11 is in good agreement with the results of *n*-hexane isomerization published recently by Hoffmeister and Butt (30). Fission of the hydrocarbon molecule, predominantly to C_3 and C_4 compounds, competes with isomerization and, as expected, is positively influenced by the increase in the temperature of reaction from 603 to 653 K. The cracking tendency clearly predominates with the SAPO-5 catalyst.

The analysis of the ice-trapped reaction product by capillary gas chromatography has shown that the condensed liquid phase contains 78 chromatographically separated components. Sixty of them could be identified with the aid of C_3 to C_7 model hydrocarbons. With all catalyst samples, the portion of the C_7 compounds including nonreacted *n*-heptane amounts to ca. 99% of the total liquid product. Among the heptanes, the thermodynamically favored monobranched 2- and 3-methylhexanes are the preferred isomers (Table 8). 2,3-Dimethylpentane, the third component prominent in the state of thermodynamic equilibrium (with a portion of 22.8 vol% at 653 K), and the tribranched 2,2,3-trimethylbutane are present in minor amounts only. Heptenes, cyclic paraffins, and olefins could be detected in traces, the portion of any of the

TABLE 6

Stoichiometry of SAPO Samples

Sample	Composition of the unit cell derived from TPDA	Atomic ratios found by chemical analysis Al : P : Si			Molar content of non-SAPO oxides per unit cell Al_2O_3	SiO_2
SAPO-17	$(Al_{18}P_{17.5}Si_{0.5}O_{72})$	18.2	17.5	1.1	0.1	0.6
SAPO-11	$(Al_{20}P_{19.5}Si_{0.5}O_{80})$	25.0	19.5	1.0	2.5	0.5
SAPO-31	$(Al_{18}P_{17.7}Si_{0.3}O_{72})$	25.0	17.7	2.3	3.5	2.0
SAPO-5	$(Al_{12}P_{11.7}Si_{0.3}O_{48})$	12.4	11.7	1.2	0.2	0.9

TABLE 7

Isomerization of *n*-Heptane

	Conversion of *n*-heptane (%)	Selectivity of iso-heptanes (%)	Conversion of *n*-heptane (%)	Selectivity of iso-heptanes (%)	Temperature of reaction (K)
8-membered oxygen rings:	SAPO-17		$AlPO_4$-17		
	7.6	78.8	1.3	80.5	603
	19.2	78.3	9.8	73.8	653
10-membered oxgen rings:	SAPO-11		$AlPO_4$-11		
	74.2	93.2	11.0	90.1	603
	82.6	67.3	39.9	85.1	653
12-membered oxygen rings:	SAPO-5		$AlPO_4$-5		
	23.5	15.4	12.6	45.0	603
	49.3	5.7	24.6	26.2	653
12-membered oxygen rings:	SAPO-31		$AlPO_4$-31		
	72.1	93.8	15.3	90.2	603
	75.4	73.0	51.8	86.7	653

Note. Conditions: catalyst, 65 mass% of molecular sieve + 35 mass% of Aerosol-200; Pd content, 0.1 mass%; catalyst weight, 4.1 g = 10.0 ml; gas feed, 1.11 ml//; $c_{n\text{-heptane}}$, 15 vol% in hydrogen.

individual compounds not exceeding 0.02 mass%. Toluene concentration is low. Apparently, dehydrocyclization can be considered a side reaction. The nearly identical selectivities of branched heptane isomers for all SAPO catalysts indicate that effects of shape selectivity are absent. Differences in the structures of the molecular sieves apparently do not seriously influence the step of isomerization.

TABLE 8

Selectivities (in %)

Product	Catalyst			
	SAPO-5	SAPO-17	SAPO-11	SAPO-31
Ethane	0.18	0.31	0.26	0.25
Ethene	0.29	0.10	0.19	0.20
Propane	35.29	8.53	10.46	8.88
Propene	0.86	0.51	0.51	0.14
Butanes	41.67	10.83	13.66	11.67
Butenes	6.29	1.28	3.78	0.84
Pentanes	8.12	0.48	2.73	0.97
Hexanes	1.63	0.27	1.07	3.90
2-methylhexane	1.93	31.23	27.92	32.00
3-methylhexane	2.52	35.16	30.14	31.51
3-ethylpentane	0.28	3.13	2.15	1.77
2,2-dimethylpentane	0.12	1.14	0.98	0.77
2,3-dimethylpentane	0.59	4.14	3.45	4.48
2,4-dimethylpentane	0.23	2.03	2.09	2.07
3,3-dimethylpentane	0.12	0.97	0.57	0.60
2,2,3-butane	0.00	0.09	0.03	0.07
Toluene	0.02	1.41	0.37	2.95

Note. Conditions: reaction feed, 15 vol% of *n*-heptane in hydrogen; feed rate, 1.11 ml/s; catalyst volume, 10 ml; reaction temperature, 653 K.

The different activities within the SAPO series cannot be understood as a result of differences in their Brønsted acidity. As is clearly shown by TPDA, the number of strong acid sites per unit cell lies between 0.3 and 0.5 for all samples, even the less active SAPO-5 and SAPO-17 showing values in the upper range. Their lower activity, however, is in line with the IR OH vibration spectra recorded after the adsorption of *n*-heptane. With SAPO-5 and SAPO-17, the portion of bridged hydroxyl groups not accessible to *n*-heptane is relatively high (Fig. 3). Hence, only a small portion of Brønsted acid sites is able to take part in the reaction. In addition, the lower catalytic activities of the highly microporous SAPO-17 and $AlPO_4$-17 samples find an explanation in the relatively small pore openings (eight-membered oxygen pore rings) of the molecular sieve framework.

The pronounced ability of SAPO-5 to catalyze the cracking of *n*-heptane is highly surprising. The selectivities of cracking products and the high rate of catalyst deactivation are similar to values found with Y-zeolite catalysts (31). Data from IR spectroscopy and TPDA, however, argue against the existence of Brønsted sites of substantially higher acidic strength. The selectivity behavior may be explained by the reduced accessibility of the bridged hydroxyl groups of the molecular sieve framework (Figs. 3 and 5); interaction of *n*-heptene formed in the primary step of dehydrogenation at the Pd sites with the sites catalyzing isomerization into iso-olefins is hindered. *n*-Heptene molecules are perhaps more easily sub-

mitted to competing reactions at other active sites. Enhanced cracking properties of SAPO-5 could be confirmed by the results found in the conversion of *n*-heptene.

In additional experiments, heptene-1 in nitrogen was reacted over Pd-free varieties of SAPO-5 and, for comparison, over SAPO-11 catalysts (Table 9). With SAPO-11, selectivity values for the heptene isomers in the initial stages of reaction are definitely higher. With SAPO-5, dominant reactions are the cracking of heptenes and the hydride transfer (formation of saturated cracked aliphatics). The source of the hydrogen, necessary for the hydride transfer, is the formation of coke rather than aromatization. Deposition of carbonaceous compounds on the catalyst causes deactivation, which is expressed by losses in activity as the reaction proceeds. A comparison of the experimental data in Table 9 reveals that the rate of deactivation is evidently much higher with SAPO-5. Assumedly, the reduced accessibility of SAPO-5 Brønsted acid sites increases the changes of acid sites of different types, e.g., Lewis sites, to take part in the reaction of the intermediately formed *n*-heptenes. Lewis sites, however, are known to catalyze favorably cracking reactions associated with the formation of coke and hydrogen transfer, as was described recently (32) for the conversion of *n*-octane over H-mordenite.

TABLE 9

Reaction of *n*-Heptene

	Time on Stream (h)			
	0.5	1.0	1.5	2.5
SAPO-11				
Conversion of *n*-heptene (%)	58.4	47.9	45.6	44.7
Selectivities (%)				
Heptene isomers	34.0	43.9	51.3	56.1
Heptane isomers	22.6	23.1	14.6	12.7
C_3/C_4 aliphatics	34.9	28.3	29.3	27.0
Hydride transfer (%)				
C_7 aliphatics	18.4	13.1	7.9	6.6
C_3/C_4 aliphatics	8.1	5.1	4.5	4.3
	Time on stream (h)			
	0.5	1.0	2.0	—
SAPO-5				
Conversion of *n*-heptene (%)	87.8	16.4	11.3	—
Selectivities (%)				
Heptene isomers	7.3	44.6	51.3	—
Heptane isomers	27.0	24.5	21.2	—
C_3/C_4 aliphatics	48.7	20.4	18.6	—
Hydride transfer (%)				
C_7 aliphatics	56.0	4.2	2.5	—
C_3/C_4 aliphatics	49.9	44.0	44.3	—

Note. Conditions: gas feed, 0.56 ml/s; $c_{n\text{-heptene}}$, 10 vol%; cat. volume, 10 ml; temperature, 548 K.

CONCLUSIONS

The catalytic behavior of molecular sieve catalysts not only is a function of the number and the acidic strength of their active sites, but is substantially influenced by the size of the pore apertures and the location of the catalytically active hydroxyl groups. If they are located outside the main channels, they may be unable to interact with the reactants. It is apparent that the geometry of the channel system of the molecular sieve is not only of importance for the transport of reactant and product molecules, but exerts a more subtle influence on the catalytic process.

Experimental product distributions can be interpreted in terms of the existence of a series of reaction pathways for the primarily formed normal olefins. A dominant reaction which proceeds parallel to the isomerization is the cracking of the intermediate olefin. Due to the presence of free hydrogen in the reacting system, hydride transfer and the formation of carbonaceous deposits are suppressed but cannot be completely avoided.

To synthesize SAPOs, which are highly active and fairly selective catalyst components in the isomerization of normal alkanes, it seems important to find the right combination of the number of Brønsted acid sites and their ability to interact with the intermediately formed olefins. Reduced accessibility to those sites may increase the probability of undesired reactions, above all the formation of cracked products.

As di- and tri-branched isomers are present only in minor quantities, it can be concluded that irrespective of the type of SAPO, *n*-heptenes are submitted predominantly to only one branching reaction at the acid sites between dehydrogenation and rehydrogenation of the Pd sites. For the isomerization of *n*-heptane, clear influences of the structure and the apertures of the pore system on the distribution among the isomerized compounds cannot be detected. Perhaps formation of compounds with more than one branching of the carbon chain is enhanced if the metallic sites present within the pore system of the molecular sieve are less numerous or less active.

$AlPO_4$-based catalysts are less active in all cases. The level achievable for the conversion of *n*-heptane, however, indicates that the acid strength of their P–OH groups is sufficient to catalyze the isomerization of *n*-heptene formed intermediately in the sequence of the reaction steps.

ACKNOWLEDGMENTS

The authors thank Dr. U. Lohse for the synthesis of SAPO-17 and $AlPO_4$-17 and for the organization of the chemical analysis for all molecu-

lar sieve samples. The XRD characterization of the samples by U. Steinike and the staff of the X-ray Analytical Laboratory is greatly appreciated.

REFERENCES

1. Miller, S. J., U.S. Patent 5,149,421 (1992).
2. Alvarez, F., Ribeiro, F. R., Gianetto, C., Chevalier, F., Pérot, G., and Guisnet, M., *in* "Zeolites, Facts, Figures, Future" (P. A. Jacobs, and R. A. van Santen, Eds.), Studies in Surface Science and Catalysis, Vol. 49, p. 1339. Elsevier, Amsterdam, 1989.
3. Weitkamp, J., and Ernst, S., *in* "Catalysis 1987" (J. W. Ward, Ed.), Studies in Surface Science and Catalysis, Vol. 38, p. 367. Elsevier, Amsterdam, 1988.
4. Weitkamp, J., and Ernst, S., *Catal. Today* **3,** 451 (1987).
5. Ernst, S., Kumar, R., Neuber, M., and Weitkamp, J., *in* "Characterization of Porous Solids" (K. K. Unger, J. Rouquerol, K. S. W. Sing, and H. Kral, Eds.), Studies in Surface Science and Catalysis, Vol. 39, p. 531. Elsevier, Amsterdam, 1988.
6. Kumar, R., Ernst, S., Kokotailo, G. T., and Weitkamp, J., *in* "Innovation in Zeolite Material Science" (P. J. Grobet, W. J. Mortier, E. F. Vansant, and G. Schulz-Ekloff, Eds.), Studies in Surface Science and Catalysis, Vol. 37, p. 451. Elsevier, Amsterdam, 1988.
7. Alvarez, F., Gianetto, G., Guisnet, M., and Pérot, G., *Appl. Catal.* **34,** 353 (1987).
8. Leglise, J., Chambellan, A., and Cornet, D., *Appl. Catal.* **69,** 15 (1991).
9. Fujimoto, K., Maeda, K., and Aimoto, K., *Appl. Catal. A Gen.* **91,** 81 (1992).
10. Martens, J. A., Tielen, M., Jacobs, P. A., and Weitkamp, J., *Zeolites* **4,** 98 (1984).
11. Martens, J. A., and Jacobs, P. A., *Zeolites* **6,** 334 (1986).
12. Lok, B. M., Messina, C. A., Patton, R. L., Gajek, R. T., Cannan, T. R., and Flanigen, E. M., U.S. Patent 4,440,871 (1984).
13. Zubowa, H.-L., Alsdorf, E., Fricke, R., Neissendorfer, F., Richter-Mendau, J., Schreier, E., Zeigan, P., and Zibrowius, B., *J. Chem. Soc., Faraday Trans.* **86,** 2307 (1990).
14. Dubinin, M. M., and Stöckli, H. F., *J. Colloid Interface Sci.* **75,** 34 (1980).
15. von Ballmoos, R., and Higgins, J. B., *Zeolites* **10,** 5 (1990).
16. Martens, J. A., Grobet, P. J., and Jacobs, P. A., *J. Catal.* **126,** 299 (1990).
17. Ojo, A. F., Dwyer, J., Dewing, J., O'Malley, P. J., and Nabhan, A., *J. Chem. Soc. Faraday Trans.* **88,** 105 (1992).
18. Jahn, E., Müller, D., and Becker, K., *Zeolites* **10,** 151 (1990).
19. Finger, G., and Kornatowski, J., *Zeolites* **10,** 615 (1990).
20. Wilson, S. T., Lok, B. M., Messina, C. A., Cannan, T. R., and Flanigen, E. M., *in* "Intrazeolite Chemistry" (G. D. Stucky and F. G. Dwyer, Eds.), ACS Symposium Series, Vol. 218, p. 79. Amer. Chem. Soc., Washington, DC, 1983.
21. Hedge, S. G., Ratnasamy, P., Kustov, L., and Kazansky, V. B., *Zeolites* **8,** 137 (1988).
22. Zibrowius, B., Löffler, E., Hunger, M., *Zeolites* **12,** 167 (1992).
23. Ward, J. W., *in* "Molecular Sieve Zeolites I" (F. R. Gould, Ed.), Advances in Chemistry Series, Vol. 101, p. 380. Amer. Chem. Soc., Washington, DC, 1970.
24. Halik, C., Lercher, J. A., Mayer, H. J., *J. Chem. Soc. Faraday Trans.* **84,** 4457 (1988).
25. Öhlmann, G., Jerschkewitz, H.-G., Lischke, G., Parlitz, B., Richter, M., and Eckelt, R., *Z. Chem.* **28,** 161 (1988).
26. Lok, B. M., Messina, C. A., Patton, R. L., Gajek, R. T., Cannan, T. R., and Flanigen, E. M., *J. Amer. Chem. Soc.* **106,** 6092 (1984).
27. Alsdorf, E., Feist, M., Fichtner-Schmittler, H., Jerschkewitz, H.-G., Lohse, U., and Parlitz, B., *J. Therm. Anal.* **33,** 691 (1988).
28. Parlitz, B., Lohse, U., and Schreier, E., *Microporous Mater.* **2,** 223 (1994).
29. Jänchen, J., Penchev, V., Löffler, E., Parlitz, B., and Stach, H., *Collect. Czech Chem. Commun.* **57,** 826 (1992).
30. Hoffmeister, M., and Butt, J. B., *Appl. Catal. A Gen.* **82,** 169 (1992).
31. Wang, Q. L., Giannetto, G., and Guisnet, M., *J. Catal.* **130,** 471 (1991).
32. Abbot, J., and Guerzoni, F. N., *Appl. Catal. A Gen.* **85,** 173 (1992).